Journal of Magnetic Resonance 287 (2018) 91–98

Contents lists available at ScienceDirect

Journal of Magnetic Resonance

journal homepage: www.elsevier.com/locate/jmr

Spin-echo based diagonal peak suppression in solid-state MAS NMR homonuclear chemical shift correlation spectra

Kaiyu Wang [a,b], Zhiyong Zhang [c], Xiaoyan Ding [d], Fang Tian [d], Yuqing Huang [b], Zhong Chen [b], Riqiang Fu [a,*]

[a] National High Magnetic Field Lab, 1800 East Paul Dirac Drive, Tallahassee, FL 32310, USA
[b] Department of Electronic Science, Fujian Provincial Key Laboratory of Plasma and Magnetic Resonance, Xiamen University, Xiamen, Fujian 361005, China
[c] Department of Chemical Physics, Weizman Institute of Science, Rehovot 76100, Israel
[d] Department of Biochemistry and Molecular Biology, Pennsylvania State University, Hershey, PA 17033, USA

ARTICLE INFO

Article history:
Received 12 November 2017
Revised 20 December 2017
Accepted 24 December 2017
Available online 28 December 2017

Keywords:
Diagonal peak suppression
Spin echo
^{13}C–^{13}C chemical shift correlation spectra
Solid-state MAS NMR
Data processing

ABSTRACT

The feasibility of using the spin-echo based diagonal peak suppression method in solid-state MAS NMR homonuclear chemical shift correlation experiments is demonstrated. A complete phase cycling is designed in such a way that in the indirect dimension only the spin diffused signals are evolved, while all signals not involved in polarization transfer are refocused for cancellation. A data processing procedure is further introduced to reconstruct this acquired spectrum into a conventional two-dimensional homonuclear chemical shift correlation spectrum. A uniformly ^{13}C, ^{15}N labeled Fmoc-valine sample and the transmembrane domain of a human protein, LR11 (sorLA), in native *Escherichia coli* membranes have been used to illustrate the capability of the proposed method in comparison with standard ^{13}C–^{13}C chemical shift correlation experiments.

1. Introduction

In a homonuclear chemical shift correlation spectrum, diagonal peaks are usually much more intense than cross peaks. While cross peaks contain all relevant information about distance restraints among nuclei being investigated, strong diagonal peaks provide little additional information but pose nuisances as they would bury weak cross peaks close-by. For instance, in ^{13}C-^{13}C chemical shift correlation experiments commonly used for protein structure elucidations, the cross peaks between Cα carbons and between aliphatic carbons from different residues are often difficult, if not impossible, to identify because they are so close to the strong diagonal signals. In particular, for *in situ* structural characterization of membrane proteins in their native membrane environments, ^{13}C-labeled lipids contribute a large portion to the diagonal peaks. Furthermore, the strong diagonal signals often cause t_1-noise and artifacts along the indirect dimension [1,2]. Therefore, suppressing diagonal peaks in the homonuclear correlation spectra is critical to unearth these useful but buried cross peaks for structural studies.

The simplest way to suppress diagonal signals is to multiply the 2D spectrum through data processing with a window function that is zero on the diagonal. But this is not practical since the breath of the diagonal signals may still overlap the nearby cross peaks. Several experimental strategies have been proposed in solution NMR for diagonal peak suppression in correlation experiments. One approach relied on spatially selective excitation accompanied with the suppression of magnetization that did not make any polarization transfer to other frequencies during the mixing process [1]. However, this method inherently reduced spectral sensitivity due to the use of slice selective excitation. Another approach to suppress the diagonal signals was based on the subtraction of two spectra, one being the normal spectrum, while the other containing only the diagonal peaks obtained separately from modified pulse sequences [3,4]. Inevitably, this approach required a high level of reproducibility and no significant relaxation during the mixing time. Diagonal peaks can also be suppressed by selecting magnetization transfer pathways where the spin-state was changed [5–8]. Unfortunately, this method is limited to TROSY-type spectra and ^{15}N-bound protons in large proteins subject to the TROSY effect. Recently, a generally applicable method for diagonal peak suppression was introduced by employing twin indirect evolution periods (t_1) to establish a spin echo [9] and a 90° pulse to tilt those non-exchanged signals (i.e. leading to the diagonal peaks) into the unobservable longitudinal direction [2,10]. It was demonstrated that the diagonal peak intensities could be suppressed by as much as 97% compared to that in the normal homonuclear correlation experiment. The disadvantage of this method appeared to be the unusual appearance of the resulting spectra with chemical shift

* Corresponding author.
E-mail address: rfu@magnet.fsu.edu (R. Fu).

https://doi.org/10.1016/j.jmr.2017.12.019
1090-7807/

differences of the correlated spins lying along the indirect dimension, making it difficult to establish the correlations between resonances as illustrated in conventional homonuclear chemical shift correlation spectra.

In solid-state NMR, the pure-exchange spectroscopy [11,12] generates a sine square function of the chemical shift difference between two spins involving in an exchange process. This sine square function becomes null when the chemical shift difference is zero and is used to modulate/multiply the resulting spectra such that the diagonal signals are removed. However, this method would also greatly suppress those signals close to the diagonal axis, because their chemical shift difference is small that its sine square modulation becomes almost zero. On the other hand, double-quantum (DQ) filtering is a common and effective method to suppress any uncoupled signals, such as from natural abundance signals or from membrane-mimetic environments and lipids that support membrane proteins [13–15]. For instance, the DQ filtered correlation spectroscopy (DQF-COSY) can be used to obtain correlations between coupled spins in a system without having any unwanted background signals [16], but their diagonal peaks remain. INADEQUATE [16] is another method utilizing DQ filtering to obtain the connectivity between coupled spins in DQ-SQ (single-quantum) correlation spectra and suppress those unwanted background signals from uncoupled spins. This method is very effective for those spins that are in close approximate, even if their chemical shifts are identical, but it does not show long-range cross peaks. EXPANSE [17] proposed by Schmidt-Rohr et al. could also be used to obtain correlations between coupled spins in a system without diagonal ridge. However, it selects only those cross peaks of protonated and nearby nonprotonated carbons. In NMR protein structural elucidations, an assignment of resonances is an essential step towards structural determination of uniformly ^{15}N and ^{13}C labeled proteins. ^{13}C-^{13}C chemical shift correlation spectroscopy is one of the key experiments in this arena to obtain distance restraints between the labeled ^{13}C sites. In this type of experiments, the correlation is typically achieved through ^{13}C-^{13}C spin diffusion [18–21] during a mixing time. Importantly, long-range inter-residue correlations, which provide crucial distance restraints, can only be achieved with long mixing times. The intense diagonal peaks and unwanted background signals from membrane-mimetic environments and lipids are usually present in such correlation spectra obscuring any cross peaks close to diagonal axis, such as between Cα carbons and between aliphatic carbons from different residues. So far, suppression of the diagonal peaks in such solid-state NMR correlation experiments has not yet been reported in the literature. Here, we demonstrate the feasibility of exploiting the spin-echo based diagonal peak suppression method [2,10] in high-resolution solid-state MAS NMR.

In solution NMR, gradient pulses are commonly used for coherence selections, as in the diagonal peak suppression method proposed by Banerjee and Chandrakumar [10]. However, in solid state NMR spectroscopy, gradient pulses are typically unavailable. In this paper, we first describe the magnetization evolving through the pulse sequence and design a complete phase cycling to achieve the specific pathway selections in order to implement such a diagonal peak suppression method. In terms of appearance, this initially obtained spectrum appears to be equivalent to a sine-modulated correlation spectrum with pairs of positive and negative peaks positioning symmetrically with respect to the spectral center in the indirect dimension. Secondly we modify the data processing procedure [22] to reconstruct the resulting spectrum into a standard chemical shift correlation spectrum, so that the correlations can be easily identified as in the conventional way. A uniformly ^{13}C, ^{15}N labeled Fmoc-valine sample and the LR11 (SorLA) transmembrane domain (TM) in native *Escherichia coli* (*E. coli*) membranes were used to demonstrate the suppression of the diagonal peaks in the ^{13}C-^{13}C correlation spectra and to discuss the performance of the method in details in comparison with the standard ^{13}C-^{13}C correlation spectra.

2. Methodology

Fig. 1 shows the pulse sequence for diagonal peak suppression (DIPS) in ^{13}C-^{13}C chemical shift correlation experiments. As the ^{13}C-^{13}C spin diffusion during the mixing time is achieved through dipolar assisted rotational resonance (DARR) [19,23], we abbreviate this diagonal peak suppression method as DIPS-DARR. After enhanced through cross polarization from ^{1}H, the ^{13}C magnetization evolves under high-power ^{1}H decoupling for a period of time t_1, followed by a 90° pulse to flip the magnetization from the xy plane to the z-axis. Along the longitudinal axis, the ^{13}C–^{13}C spin diffusion takes place during a mixing time of t_{mixing} to transfer the ^{13}C magnetization from one site to others. The spin diffusion is enhanced by a DARR irradiation on the ^{1}H channel. The magnetization is brought back to the xy plane by a second 90° pulse at the end of the mixing time and then evolves for another period of time t_1 under high-power ^{1}H decoupling. At the end of the second t_1 period, two additional 90° pulses are applied for diagonal peak suppression before the signal detection.

Here we use an *I*-*S* two-spin system for simplicity to illustrate how the diagonal peaks can be suppressed in this sequence. The *I* and *S* spins have their respective chemical shifts Ω_I and Ω_S. Assuming no J-coupling is present between these two spins, the *I* and *S* magnetizations evolved at different stages in the pulse sequence can be described in the following.

After cross polarization, we have

$$(a):\ I_X + S_X.$$

When evolving for the first t_1 period under their respective frequencies, these magnetizations become

$$(b):\ I_X\cos(\Omega_I t_1) + I_Y\sin(\Omega_I t_1) + S_X\cos(\Omega_S t_1) + S_Y\sin(\Omega_S t_1).$$

Applying a 90°$_y$ (i.e. φ_2 = y) to flip I_X and S_X components to the z-axis, we can obtain

$$(c):\ -I_Z\cos(\Omega_I t_1) - S_Z\cos(\Omega_S t_1).$$

During t_{mixing}, the magnetizations are diffused from *I* to *S* and from *S* to *I* as

$$(d):\ (-C_{II}I_Z - C_{IS}S_Z)\cos(\Omega_I t_1) + (-C_{SI}I_Z - C_{SS}S_Z)\cos(\Omega_S t_1).$$

Here, C_{ij} is the transfer coefficient from *i* to *j* spin during the mixing time. For instance, C_{IS} and C_{SI} represent the spin diffused magnetization coefficients during the mixing time from *I* to *S*

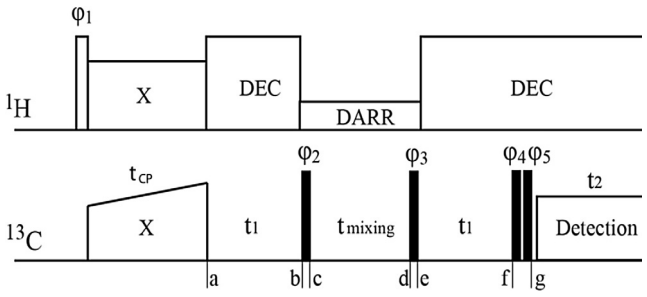

Fig. 1. Schematics of the pulse sequence used for diagonal peak suppression in 2D homonuclear correlation experiments in solid-state MAS NMR. "DEC" represents decoupling irradiation. The open rectangle in ^{1}H channel and solid rectangles in ^{13}C channel stand for 90° hard pulses. The complete phase cycling designed for this pulse sequence is listed as follows: φ_1 (y, −y), φ_2 (y, y, y, y, −x, −x, −x, −x), φ_3 (y, y, y, y, x, x, x, x, −y, −y, −y, −y, −x, −x, −x, −x), φ_4 (−x, −x, x, x), φ_5 (x), and the receiver phase (y, −y, −y, y, y, −y, −y, y, −y, y, y, −y, −y, y, −y, y).

and from S to I, respectively, while C_{II} and C_{SS} stand for the self-transfer coefficients for the I and S spin over the mixing time, which depend on their spin-lattice relaxation times as well as the amount of magnetizations diffused away from I to S and from S to I, respectively.

At the end of the mixing time, a second 90°$_y$ (i.e. $\varphi_3 = y$) flips these mixed magnetizations into the xy plane:

$$(e): \ (-C_{II}I_X - C_{IS}S_X)\cos(\Omega_I t_1) + (-C_{SI}I_X - C_{SS}S_X)\cos(\Omega_S t_1).$$

These magnetizations process for the second t_1 period at their respective frequencies leading to

$$\begin{aligned}(f): \ & -\tfrac{1}{2}C_{II}\{I_X[1+\cos(2\Omega_I t_1)] + I_Y\sin(2\Omega_I t_1)\} \\ & -\tfrac{1}{2}C_{IS}\{S_X[\cos((\Omega_I-\Omega_S)t_1)+\cos((\Omega_I+\Omega_S)t_1)] \\ & +S_Y[-\sin((\Omega_I-\Omega_S)t_1)+\sin((\Omega_I+\Omega_S)t_1)]\} \\ & -\tfrac{1}{2}C_{SS}\{S_X[1+\cos(2\Omega_S t_1)] + S_Y\sin(2\Omega_S t_1)\} \\ & -\tfrac{1}{2}C_{SI}\{I_X[\cos((\Omega_S-\Omega_I)t_1)+\cos((\Omega_S+\Omega_I)t_1)] \\ & +I_Y[-\sin((\Omega_S-\Omega_I)t_1)+\sin((\Omega_S+\Omega_I)t_1)]\}\end{aligned}$$

Clearly, for C_{II} and C_{SS}, the time-independent I_X and S_X terms correspond to the refocusing of the magnetizations I_X and S_X, while the time-dependent I_X and S_X terms evolve at their own frequencies Ω_I and Ω_S, respectively. As for the spin diffused intensities of C_{IS} and C_{SI}, their magnetizations evolve at two frequencies $(\Omega_I + \Omega_S)$ and $(\Omega_I - \Omega_S)$, i.e. the sum and difference of chemical shifts of the I and S spins. A final pair of 90° pulses with phases of $\varphi_4 = \pm x$ and $\varphi_5 = x$ serves as 180°$_x$ and 0°$_x$ pulses to change the signs of I_Y and S_Y while to keep I_X and S_X in the same direction in two consecutive scans. Therefore, those refocused magnetizations of I_X and S_X are canceled by subtraction of the two scans, so that the remaining magnetizations become:

$$\begin{aligned}(g): \ & -\tfrac{1}{2}C_{II}\{I_Y\sin(2\Omega_I t_1)\} - \tfrac{1}{2}C_{IS}\{S_Y[-\sin((\Omega_I-\Omega_S)t_1) \\ & \qquad +\sin((\Omega_I+\Omega_S)t_1)]\} \\ & -\tfrac{1}{2}C_{SS}\{S_Y\sin(2\Omega_S t_1)\} - \tfrac{1}{2}C_{SI}\{I_Y[-\sin((\Omega_S-\Omega_I)t_1) \\ & \qquad +\sin((\Omega_I+\Omega_S)t_1)]\}\end{aligned}$$

Similarly, when $\varphi_2 = -x$, $\varphi_3 = x$, $\varphi_4 = \pm x$, and $\varphi_5 = x$, the magnetizations at stage (g′) become

$$\begin{aligned}(g'): \ & \tfrac{1}{2}C_{II}\{I_Y\sin(2\Omega_I t_1)\} + \tfrac{1}{2}C_{IS}\{S_Y[\sin((\Omega_I-\Omega_S)t_1) \\ & \qquad +\sin((\Omega_I+\Omega_S)t_1)]\} \\ & +\tfrac{1}{2}C_{SS}\{S_Y\sin(2\Omega_S t_1)\} + \tfrac{1}{2}C_{SI}\{I_Y[\sin((\Omega_S-\Omega_I)t_1) \\ & \qquad +\sin((\Omega_I+\Omega_S)t_1)]\}\end{aligned}$$

Therefore, the summation of (g) and (g′) results in the magnetizations of $C_{IS}\{S_Y[\sin((\Omega_I-\Omega_S)t_1)]\} + C_{SI}\{I_Y[\sin((\Omega_S-\Omega_I)t_1)]\}$, which contain only the spin diffused signals C_{IS} from I to S and C_{SI} from S to I, both evolving sinusoidally for the t_1 period at the frequency of their chemical shift difference $(\Omega_I - \Omega_S)$.

A Fourier transform of this sine modulation $\sin((\Omega_I - \Omega_S)t_1)$ brings into a pair of peaks positioning at the frequency of $(\Omega_I - \Omega_S)$ and $(\Omega_S - \Omega_I)$ with opposite signal intensities in the indirect (i.e. F1) dimension. The resulting 2D DIPS-DARR spectrum is illustrated in Fig. 2a. For the I spin at Ω_I in the observed (i.e. F2) dimension, it correlates with a negative peak at $(\Omega_I - \Omega_S)$ and a positive peak at $(\Omega_S - \Omega_I)$ in the F1 dimension. While for the S spin at Ω_S in the F2 dimension, it correlates with a positive peak at $(\Omega_I - \Omega_S)$ and a negative peak at $(\Omega_S - \Omega_I)$ in the F1 dimension. The zero frequency in the F1 dimension, on the other hand, represents any time-independent contributions in the DIPS-DARR experiment, which corresponds to the diagonal signals in the standard ^{13}C-^{13}C DARR spectrum, as illustrated in Fig. 2b. Clearly, this DIPS-DARR spectrum is quite different from the DARR spectrum and would be difficult to analyze with the conventional approach.

To facilitate the analysis of the DIPS-DARR spectra, we introduce the reconstruction procedure [22] to convert the DIPS-DARR spectrum into the conventional DARR-style spectrum. Since the spin-diffused positive peak in the DIPS-DARR spectrum appears at $(\Omega_S - \Omega_I, \Omega_I)$, a simple operation of shifting the peak position at $(\Omega_S - \Omega_I)$ by Ω_I along the F1 dimension would make the peak appearing at (Ω_S, Ω_I), which is the cross peak position in the conventional DARR spectrum. Taking the symmetrical distribution feature of the DIPS-DARR spectrum into account, we depict a mathematical manipulation for the data reconstruction procedure

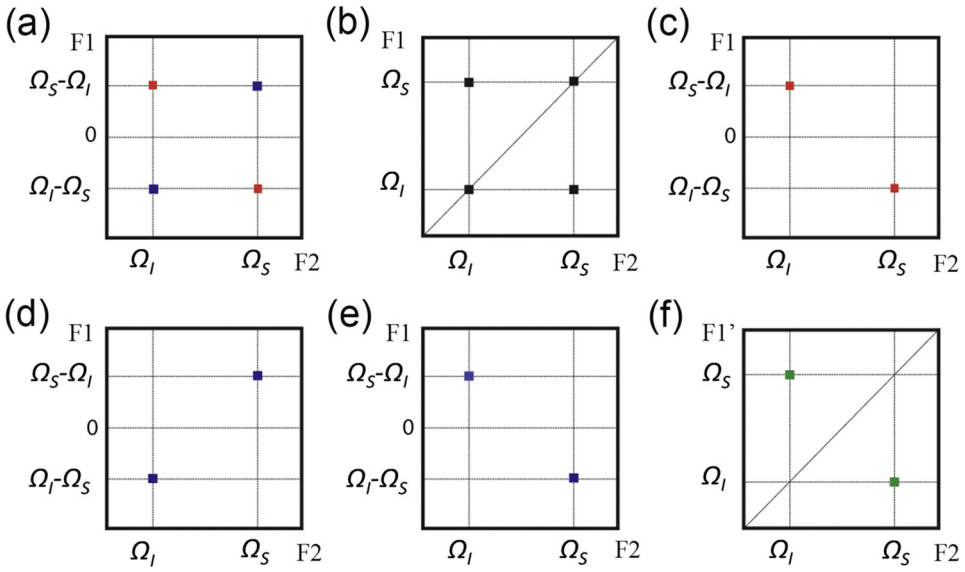

Fig. 2. Scheme of the reconstruction procedure converting the DIPS-DARR spectrum to a standard DARR spectrum. Red and blue squares represent positive and negative cross peaks, respectively. (a) DIPS-DARR spectrum. (b) Standard DARR spectrum. (c) The positive spectrum and (d) the negative spectrum extracted from the DIPS-DARR spectrum. (e) Symmetrically flipped negative spectrum along the horizontal zero-frequency line. (f) Reconstructed DIPS-DARR spectrum (green squares) after using the positive spectrum of (c) to subtract the flipped negative spectrum of (e) and then shearing the combined spectrum with process along the F1′ axis: $\Omega_1' = \Omega_1 + \Omega_2$. (For interpretation of the references to color in this figure legend, the reader is referred to the web version of this article.)

as follows: firstly, loading the DIPS-DARR spectrum into a processing program (c.f. Fig. 2a); secondly, separating the DIPS-DARR spectrum in Fig. 2a into the positive (c.f. Fig. 2c) and negative (c.f. Fig. 2d) spectra; thirdly, symmetrically flipping the negative part along the horizontal zero-frequency line, putting the negative peaks at the same position as the positive peaks in the spectrum (c.f. Fig. 2e). Finally, creating a combined spectrum by using the positive spectrum in Fig. 2c to subtract the flipped negative spectrum in Fig. 2e in order to sum up the peak intensities, and then shifting this combined spectrum through the process along the F1 dimension according to $\Omega_1' = \Omega_1 + \Omega_2$ to obtain the reconstructed DIPS-DARR spectrum, which is free of diagonal peaks (c.f. Fig. 2f).

Explicit explanation for the mathematical manipulation of $\Omega_1' = \Omega_1 + \Omega_2$ is described as follows. The spectral widths of a DIPS-DARR spectrum are SW1 in the F1 dimension and SW2 in the F2 dimension, number of points are N1 in the F1 dimension and N2 in the F2 dimension. By zero-filling N0 points into the F1 dimension, we can generate an identical digital resolution in both dimensions, i.e. Δ = SW1/(N1 + N0) = SW2/N2. Since this digital resolution Δ represents the ppm value per point, the number of points of Ω_2/Δ corresponds to a shift distance of Ω_2. Therefore, with the same digital resolution in both dimensions, shifting any position Ω_1 in the F1 dimension of the DIPS-DARR spectrum by a distance of Ω_2 can be simply achieved by moving a position (Ω_1, Ω_2) by Ω_2/Δ points along the F1 dimension to the new position at ($\Omega_1 + \Omega_2$, Ω_2) in the F1′ dimension of the newly reconstructed spectrum. Specifically, for those displayed in Fig. 2, the peak at ($\Omega_S - \Omega_I$, Ω_I) in Fig. 2d and e become peak at (Ω_S, Ω_I) in Fig. 2f, and the point at (0, Ω_S) in Fig. 2d and e become the diagonal point at (Ω_S, Ω_S), thus transferring a DIPS-DARR spectrum into a DARR-style one.

3. Experimental

^{13}C labeled Fmoc-valine was purchased from Cambridge Isotope Laboratories, Inc. and used without further purification. All NMR experiments were carried out on a Bruker Avance 600 MHz NMR spectrometer operating at the resonance frequency of 600.13 MHz for ^{1}H and 150.82 MHz for ^{13}C using a NHMFL 3.2 mm low-E double-resonance biosolids MAS probe [24]. The sample spinning rate was controlled by a Bruker pneumatic MAS unit at 14 kHz ± 3 Hz. The ^{13}C magnetization was enhanced by cross-polarization with a contact time of 1 ms, during which a ^{1}H spin-lock field of 50 kHz was used and the ^{13}C B_1 field was ramped from 38 to 56 kHz. The ^{13}C 90° pulse length used was 2.9 μs. A SPINAL64 decoupling sequence [25] with a ^{1}H B_1 filed of 78.0 kHz was used during the t_1 and t_2 dimensions. During the mixing time of t_{mixing} = 50 ms, a ^{1}H B_1 field of 14 kHz was applied for the DARR irradiation to enhance the ^{13}C-^{13}C spin diffusion. The spectral widths for the t_2 and t_1 dimensions were 100 and 60 kHz, respectively. 3072 data points were acquired in the t_2 dimensions. In the t_1 dimension, 1280 points were obtained in the DARR experiment and 640 points in the DIPS-DARR experiment so that both DARR and DIPS-DARR experiments has the same t_1 acquisition time, since the former used TPPI for quadrature detection [26] while the latter one did not use the quadrature detection in the t_1 dimension. 16 scans were used in the DARR experiments and 32 scans in the DIPS-DARR experiment, giving the same experimental time of 11.8 h for sensitivity comparison in these two experiments. The complete phase cycling designed for the DIPS-DARR experiment was listed as follows: φ_1 (y, −y), φ_2 (y, y, y, y, −x, −x, −x, −x), φ_3 (y, y, y, y, x, x, x, x, −y, −y, −y, −y, −x, −x, −x, −x), φ_4 (−x, −x, x, x), φ_5 (x), and the receiver phase of (y, −y, −y, y, y, −y, −y, y, −y, y, y, −y, −y, y, −y, y). No window functions were used in both dimensions before the data processing. The ^{13}C chemical shifts were referenced to the carbonyl carbon resonance of glycine at 178.4 ppm, relative to 4,4-di methyl-4-silapentanesulfonate sodium (DSS).

4. Results and discussion

Fig. 3a shows the ^{13}C CPMAS NMR spectrum of the Fmoc-valine sample. The isotropic chemical shifts for the five labeled ^{13}C carbons in the valine group (i.e. C′, Cα, Cβ, Cγ, and Cδ) were uniquely assigned: $\delta_{C'}$ = 178.4, $\delta_{C\alpha}$ = 59.4, $\delta_{C\beta}$ = 30.3, $\delta_{C\gamma}$ = 21.2, and $\delta_{C\delta}$ = 15.1 ppm, as labeled in the plot. With a mixing time of t_{mixing} = 50 ms used in the experiments, spin diffusion would take place among all carbons, meaning that for each carbon resonance its magnetization would spin diffuse to other four carbons. Therefore, a total of eight peaks (four positive in red and four negative in blue) are expected in the DIPS-DARR spectrum, as shown in Fig. 3b. The standard DARR correlation spectrum (c.f. Fig. 3c) clearly shows the ^{13}C-^{13}C correlations. For instance, the cross peak at ($\delta_{C\alpha}$, $\delta_{C'}$) corresponds to the correlation between the two diagonal peak positions of Cα and C′. In comparison, the DIPS-DARR spectrum presents a very different pattern. For instance, the cross peak at ($\delta_{C\alpha}$, $\delta_{C'}$) in the standard DARR spectrum appears at ($\delta_{C\alpha} - \delta_{C'}$, $\delta_{C'}$) in the DIPS-DARR spectrum, which is difficult to analyze in a straightforward manner. With a custom-written MATLAB script, the original DIPS-DARR spectrum was separated into the positive part (Fig. 3d) and the negative part. They are symmetric along the zero-frequency line in the F1 dimension. By flipping the negative part along the zero-frequency line in the F1 dimension, we can convert the negative spectrum to the same appearance as in the positive one (c.f. Fig. 3). Then the positive spectrum and the flipped negative one were subtracted to double the signal intensities. Subsequent process of shifting the combined spectrum according to the algorithm of $\Omega_1' = \Omega_1 + \Omega_2$ converted the peak positions from ($\Omega_I - \Omega_S$, Ω_S) into (Ω_I, Ω_S) and thus produced a reconstructed DARR-style spectrum, as shown in Fig. 3f. In comparison with the standard DARR spectrum in Fig. 3c, the reconstructed DIPS-DARR spectrum shows the same pattern for the cross peaks but with little diagonal peaks.

Fig. 4 shows one-dimensional slices taken from the cross peak representing the spin diffusion from Cα to C′ along the F2 dimension in different spectra. For the slice taken from the DIPS-DARR spectrum in Fig. 4a, the positive peak is the spin diffused signal from Cα to C′, while the negative peak corresponds to the signal transferred from C′ to Cα. The observed signal intensity for the positive peak is 0.24. On the other hand, the intensity for the same cross peak at ($\delta_{C\alpha}$, $\delta_{C'}$) from the reconstructed DIPS-DARR spectrum (c.f. Fig. 4b) becomes 0.47, which is about twice of the cross peak intensity from the DIPS-DARR spectrum, as expected from the reconstruction procedure, while the Cα diagonal peak intensity (as indicated in black dashed box) is as small as 0.0062. For comparison, the observed intensity for the ($\delta_{C\alpha}$, $\delta_{C'}$) cross peak (as indicated in red dashed box) in the DARR spectrum (c.f. Fig. 4c) is 0.71 with the Cα diagonal peak intensity of 0.74. Therefore, the reconstructed DIPS-DARR spectrum suppresses 99% (i.e. 1–0.0062/0.74) of the diagonal peak intensity while remains about 66% (i.e. 0.47/0.71) of the cross peak intensity. Other cross peak intensities in the reconstructed DIPS-DARR spectrum were found to be slightly over 50% compared to their counterparts in the DARR spectrum. It should be noticed that in above theoretical description of the pulse sequence in Fig. 1 the coefficient C_{IS} at the stage (d) after the mixing time corresponds to the cross peak intensity from I to S spin in the standard DARR experiments, while the coefficient becomes $C_{IS}/2$ at the stage (g) in the DIPS-DARR experiments. Therefore, cross peak intensities in the reconstructed DIPS-DARR spectrum are expected to be half of their intensities in the conventional DARR spectrum. The main advantage of the DIPS-DARR

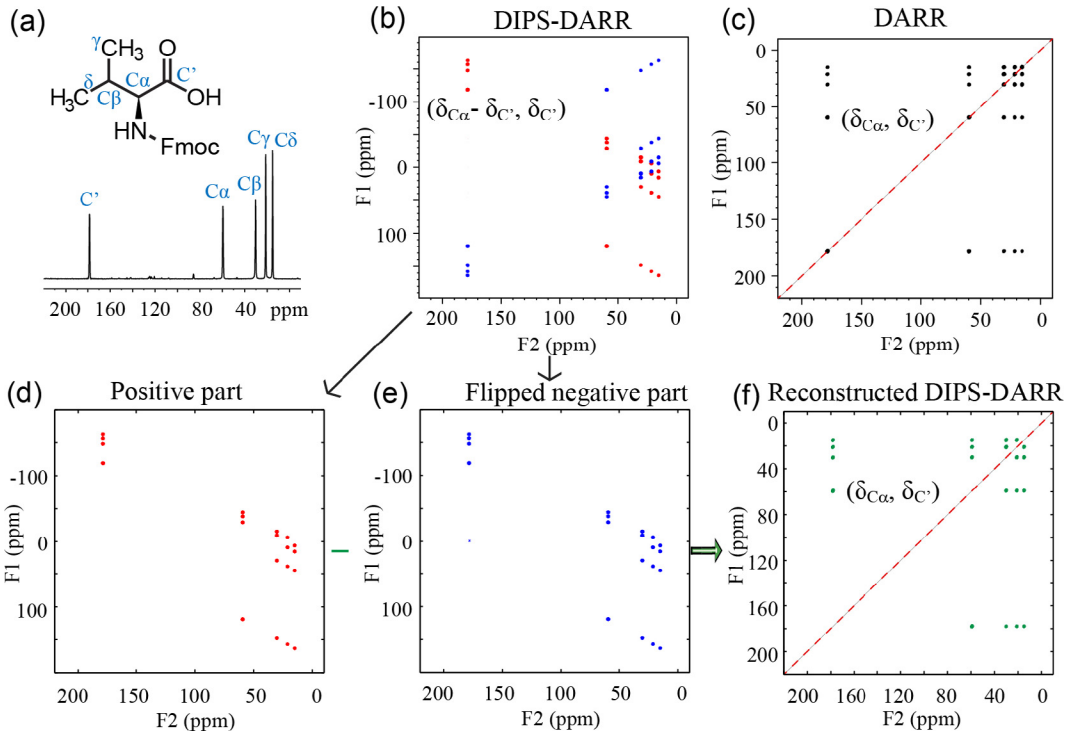

Fig. 3. Experimental results of Fmoc-valine sample and the reconstruction procedure of converting the DIPS-DARR spectrum to a standard DARR spectrum. Red and blue dots represent positive and negative cross peaks, respectively. (a) The molecular structure of Fmoc-valine and its 1D ^{13}C CPMAS spectrum. (b) The DIPS-DARR spectrum obtained by the pulse sequence in Fig. 1. (c) The standard DARR spectrum. (d) The positive spectrum extracted from the DIPS-DARR spectrum. (e) Negative spectrum extracted from Fig. 3b, symmetrically flipped along the zero frequency in the F1 dimension. (f) Reconstructed DIPS-DARR spectrum after shearing the combined spectrum, which is the subtraction of (d and e), with the process along the F1 axis: $\Omega_1' = \Omega_1 + \Omega_2$. (For interpretation of the references to color in this figure legend, the reader is referred to the web version of this article.)

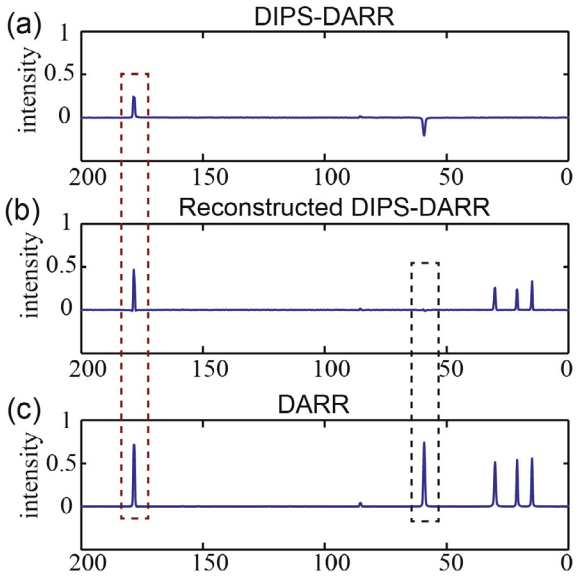

Fig. 4. One-dimensional slices taken from the cross peak between the Cα to C′ resonances along the F2 dimension in different spectra. (a) The DIPS-DARR Spectrum, (b) the reconstructed DIPS-DARR spectrum, and (c) the standard DARR spectrum. Peaks in the red dashed box are the cross peak while the peaks in the black dashed box indicate the Cα diagonal peak. (For interpretation of the references to color in this figure legend, the reader is referred to the web version of this article.)

experiment is to efficiently suppress the diagonal peaks so that any cross peaks that are close to the diagonal axis can now be identified.

In the DIPS-DARR experiment, for a given carbon its spin diffused signal intensities from other carbons are modulated sinusoidally in the t_1 dimension at the respective chemical shift differences between this carbon and others, such that a set of paired peaks with opposite signal intensities coexist along the F1 dimension. When the carbon has either the highest (c.f. $\delta_{C'}$) or the lowest (c.f. $\delta_{C\delta}$) chemical shift value than other carbons, the positive and negative peaks are located in well-separated regions, either at the upper half or at the lower half of the resulting DIPS-DARR spectrum in the F1 dimension, as shown in Fig. 3b. However, when the positive and negative peaks are not located in the well-separated regions, the spin diffused signals may interfere with each other as a result of the positive and negative contributions from different carbons. Fig. 5 shows a hypothetical extreme circumstance where three carbons sites A, B, and C are present and their chemical shifts fulfill this relationship $\Omega_A - \Omega_B = \Omega_B - \Omega_C$. When spin diffusions take place between A and B and between B and C, their standard DARR spectrum will display cross peaks between Ω_A and Ω_B as well as between Ω_B and Ω_C, as shown in Fig. 5a. For this example, the expected DIPS-DARR spectrum is shown in Fig. 5b, where the blue[1] and red colors represent the negative and positive peaks, respectively. The spin diffused signals between A and B are depicted in open squares, while the ones between B and C are indicated in open triangles. Therefore, as shown in Fig. 5b, for the B carbon at Ω_B, the negative peak spin diffused from the A carbon coincides exactly in the same position of the positive peak diffused from the C carbon in the upper half of the spectrum. Similarly, the positive peak spin diffused from the A carbon overlaps with the negative peak diffused from the C carbon in the

[1] For interpretation of color in Fig. 5, the reader is referred to the web version of this article.

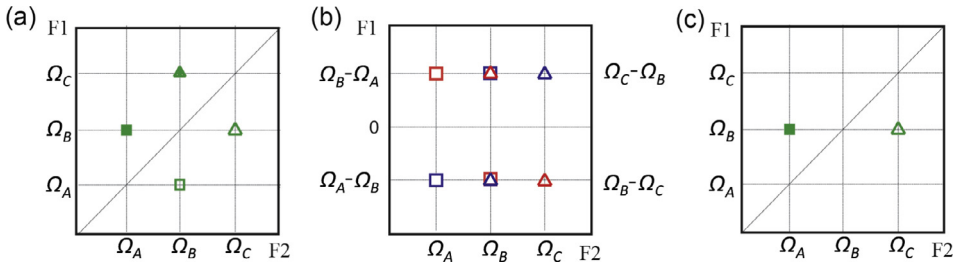

Fig. 5. (a) The standard DARR correlation spectrum of a three-spin system where B is correlated to both A and C. (b) The expected DIPS-DARR spectrum. (c) The reconstructed DIPS-DARR spectrum from (b) when the spin diffusion transfers from A to B and from C to B are the same.

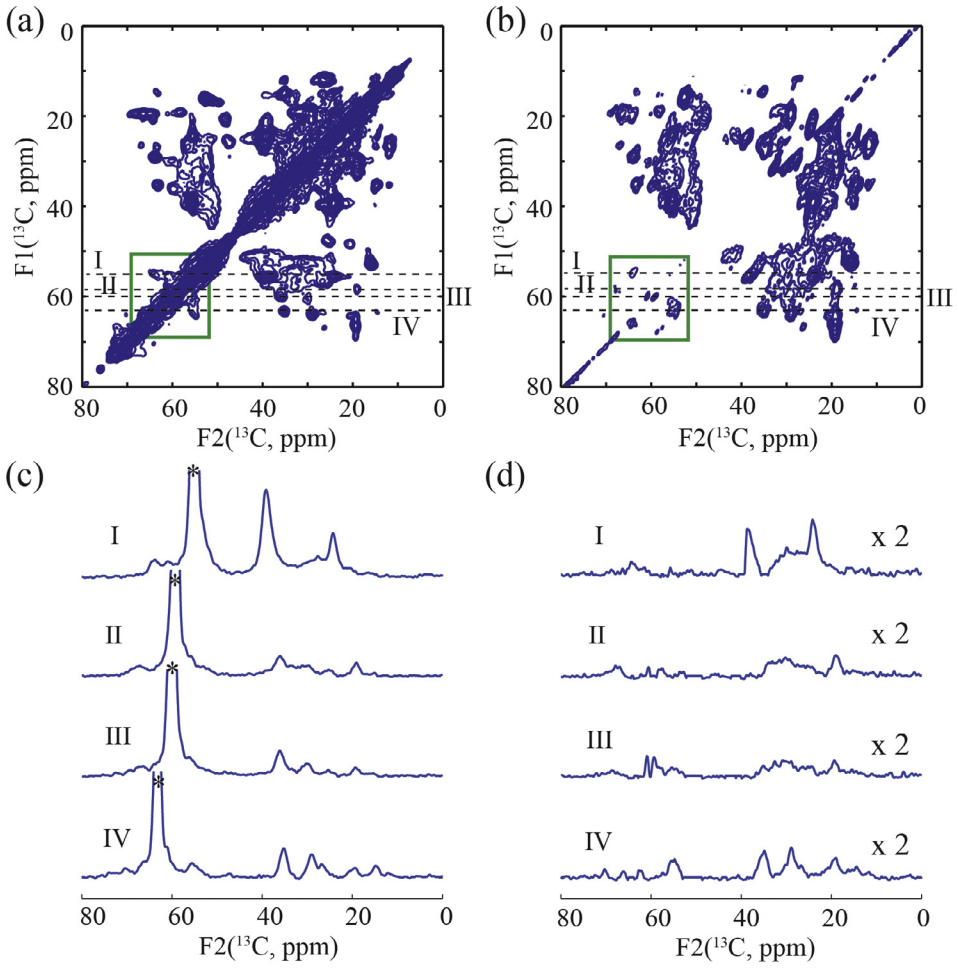

Fig. 6. Experimental results of ^{13}C, ^{15}N-labeled LR11 TM in native *E. coli* inner membrane vesicles. (a) The standard DARR spectrum. (b) The reconstructed DIPS-DARR spectrum. One-dimensional slices in (c) and (d) were taken along the black dashed lines at 55.1 ppm (I), 59.1 ppm (II), 59.9 ppm (III), 63.1 ppm (IV) from (a and b), respectively. The truncated peaks labeled with asterisks in (c) are their corresponding diagonal peaks. Both the standard DARR spectrum and the reconstructed DIPS-DARR spectrum were recorded at 280 K on a Bruker Avance 600 MHz NMR spectrometer. The sample spinning rate was 12 kHz ± 3 Hz. The CP condition was the same as in Fig. 3, while the ^{13}C 90° pulse length used was 3.4 μs. The spectral widths for the t_2 and t_1 dimensions were 100 and 60 kHz, respectively. In the DARR experiment, 128 scans were used to accumulate each of 512 t_1 increments, while in the DIPS-DARR experiment, 256 scans were used to accumulate each of 256 t_1 increments. A 10 ms mixing time was used in both experiments. A Gaussian window function (LB = −20 Hz and GB = 0.1) was applied in both dimensions during the data processing.

lower half of the spectrum. If the spin diffusion transfers from A to B and from C to B are the same, no peaks should be expected at Ω_B along the F1 dimension, as if no spin diffusion is taken place either from A to B or from C to B. However, in the reconstructed DIPS-DARR spectrum as shown in Fig. 5c, it is still possible to trace the cross peaks between B and A as well as between B and C.

Next we applied this method to suppress diagonal peaks in the ^{13}C-^{13}C correlation spectrum of LR11 (SorLA) TM in the native *E. coli* membrane vesicles. LR11 is a type-I transmembrane protein involved in the development of Alzheimer's disease (AD), which causes a gradual loss of memory and general cognitive decline in human being. Here the LR11 TM domain, whose amino acid fragment sequence is RSTDVAAVVV PILFLILLSL GVGFAILYTK, was expressed in *E. Coli* using a MBP-fusion expression vector, as described in the literature [27]. Fig. 6 shows the ^{13}C-^{13}C correlation spectra of the uniformly ^{13}C, ^{15}N-labeled LR11 TM in native *E. coli* membrane vesicles. In the standard DARR spectrum in Fig. 6a, the strong diagonal peaks include signals from ^{13}C-labeled proteins

and lipids, and obscure cross peaks that are close to the diagonal axis, especially in the 20–40 ppm region. For comparison, in the reconstructed DIPS-DARR spectrum in Fig. 6b the intense diagonal peaks are greatly reduced. As a result, some cross peaks nearby the diagonal axis can be readily identified such as those in the green boxed region as well as in the region of 20–30 ppm. Fig. 6c shows the slices taken along the black dashed lines from Fig. 6a, and Fig. 6d has the same slices taken from Fig. 6b. It is obvious that the strong diagonal peaks as indicated by the asterisks in Fig. 6c are sufficiently suppressed by the proposed method as in Fig. 6d, while the off-diagonal peaks remain. For the slice III, the diagonal peak position is at around 59.9 ppm. In Fig. 6c, the base of the diagonal peak appears to be broad, such that no apparent off-diagonal peaks could be observed. However, with the suppression of the strong diagonal peak, we could clearly observe the two distinct peaks at 59.6 and 60.9 ppm as shown in Fig. 6d. This may be a good example to illustrate the fundamental difference between the pure-exchange spectroscopy and this spin-echo based DIPS-DARR method. In the pure-exchange spectroscopy [11], the diagonal peaks are suppressed by generating a sine square modulation of the chemical shift difference that has a null point at the diagonal (i.e. corresponding to no chemical shift difference). When a signal is close to the diagonal, their chemical shift difference is small. As a result, the sine square modulation becomes very little with a limited modulation period in the xy plane (due to the T_2 effect), such that the cross peak between these two spins is also dramatically suppressed. While in the spin-echo based DIPS-DARR experiment, all signals that are not involved in spin diffusion are refocused by the spin echo sequence and thus eventually suppressed, but the spin diffused signals evolve and lead to the cross peaks in the reconstructed DIPS-DARR spectra. Such spin diffused signals are generated via spin diffusion during a longitudinal mixing time, which could be very long (due to the T_1 effect). The spin diffusion could take place as long as the two spins experience any difference in magnetization along the longitudinal axis during the mixing time, even when they have identical chemical shift values.

It is worth noting that the pattern of cross peaks in the upper left side is similar in both spectra, owing to the fact that the chemical shifts of all Cα carbons are in the left side of the other aliphatic carbons. As discussed earlier, the spin-diffused signals from the aliphatic carbons have the same sign (either positive or negative) in the region, so that no signal cancelation takes place in this region. However, in other regions, the spin diffused signals inevitably alter their respective intensities due to the fact that the positive and negative contributions from different carbons overlap, causing some differences in the patterns of the cross peaks. This shortcoming is associated with the sine modulation of the chemical shift difference between two spins involving in spin diffusion. The possibility of introducing a cosine modulation, similar to the pure-exchange spectroscopy [11], to utilize the quadrature detection in the t_1 dimension would solve this issue, which will be investigated in the future. Nevertheless, the diagonal peaks are effectively suppressed by this spin-echo based method.

5. Conclusion

An effective diagonal peak suppression method has been proposed in high-resolution solid-state MAS NMR homonuclear chemical shift correlation experiments. The spin-echo based diagonal peak suppression method, originated from solution NMR experiments, is adapted for the first time in solid-state MAS NMR to eliminate all signals that do not make polarization transfers and to evolve only those spin diffused signals in the indirect dimension. This initially obtained spectrum, in terms of appearance, is equivalent to a sine-modulated correlation spectrum with pairs of positive and negative peaks positioning symmetrically with respect to the spectral center in the indirect dimension. A data processing procedure is then introduced to reconstruct the resulting spectrum into a conventional-like ^{13}C-^{13}C correlation spectrum, so that the homonuclear correlation spectrum free of diagonal peaks could be obtained in solid-state MAS NMR. By using the uniformly labeled Fmoc-valine sample as an example, we have demonstrated experimentally that 99% of the diagonal peak intensities could be suppressed, while at least 50% of the cross peak intensities remain in the reconstructed spectrum. Thus, it is anticipated that this efficient diagonal peak suppression method offers an opportunity to identify cross peaks that are close to the diagonal axis, such as between Cα carbons and between aliphatic carbons from different residues in membrane proteins, in the homonuclear chemical shift correlation spectra, which will be beneficial for resonance assignments and structural characterizations.

Acknowledgments

All NMR experiments were carried out at the National High Magnetic Field Lab (NHMFL) supported by the NSF Cooperative agreement no. DMR-1157490 and the State of Florida. This work was also in part supported by National Natural Science Foundation of China No. U1632274 and by the National Institute of Health NIGMS (R01GM105963 to F.T.). KYW thanks to the financial support from the China Scholarship Council for visiting the NHMFL.

References

[1] S. Glanzer, E. Schrank, K. Zangger, A general method for diagonal peak suppression in homonuclear correlated NMR spectra by spatially and frequency selective pulses, J. Magn. Reson. 232 (2013) 1–6.
[2] G.S. Harbison, J. Feigon, D.J. Ruben, J. Herzfeld, R.G. Griffin, Diagonal peak suppression in 2D-NOE spectra, J. Am. Chem. Soc. 107 (1985) 5567–5569.
[3] K. Nagayama, Y. Kobayashi, Y. Kyogoku, Difference techniques to pick up cross-peaks and suppress auto-peaks in two-dimensional shift-correlated and two-dimensional exchange NMR spectroscopies, J. Magn. Reson. 51 (1983) (1969) 84–94.
[4] J. Cavanagh, J. Keeler, Complete suppression of diagonal peaks in COSY spectra, J. Magn. Reson. 71 (1987) (1969) 561–567.
[5] T. Diercks, V. Truffault, M. Coles, O. Millet, Diagonal-Free 3D/4D HN, HN-TROSY-NOESY-TROSY, J. Am. Chem. Soc. 132 (2010) 2138–2139.
[6] A. Meissner, O.W. Sørensen, Suppression of diagonal peaks in TROSY-type ^{1}H NMR NOESY spectra of ^{15}N-labeled proteins, J. Magn. Reson. 140 (1999) 499–503.
[7] A. Meissner, O.W. Sørensen, Three-dimensional protein NMR TROSY-type ^{15}N-resolved $^{1}H^{N}$–$^{1}H^{N}$ NOESY spectra with diagonal peak suppression, J. Magn. Reson. 142 (2000) 195–198.
[8] G. Zhu, Y. Xia, K.H. Sze, X. Yan, 2D and 3D TROSY-enhanced NOESY of ^{15}N labeled proteins, J. Biomol. NMR 14 (1999) 377–381.
[9] E.L. Hahn, Spin echoes, Phys. Rev. 80 (1950) 580–594.
[10] A. Banerjee, N. Chandrakumar, Two-dimensional nuclear magnetic resonance: exploiting spin echoes to maximize information content by suppression of diagonal peaks in homonuclear experiments, J. Phys. Chem. A 119 (2015) 482–487.
[11] E.R. deAzevedo, T.J. Bonagamba, K. Schmidt-Rohr, Pure-exchange solid-state NMR, J. Magn. Reson. 142 (2000) 86–96.
[12] T. Vosegaard, N.C. Nielsen, Improved pulse sequences for pure exchange solid-state NMR spectroscopy, Magn. Reson. Chem. 42 (2004) 285–290.
[13] J.J. Lopez, C. Kaiser, S. Shastri, C. Glaubitz, Double quantum filtering homonuclear MAS NMR correlation spectra: a tool for membrane protein studies, J. Biomol. NMR 41 (2008) 97–104.
[14] M. Hong, Solid-state dipolar INADEQUATE NMR spectroscopy with a large double-quantum spectral width, J. Magn. Reson. 136 (1999) 86–91.
[15] D. Huster, L. Xiao, M. Hong, Solid-state NMR investigation of the dynamics of the soluble and membrane-bound colicin Ia channel-forming domain, Biochemistry 40 (2001) 7662–7674.
[16] J. Keeler, Understanding NMR Spectroscopy, second ed., Wiley, 2010.
[17] R.L. Johnson, J.M. Anderson, B.H. Shanks, X. Fang, M. Hong, K. Schmidt-Rohr, Spectrally edited 2D ^{13}C–^{13}C NMR spectra without diagonal ridge for characterizing ^{13}C-enriched low-temperature carbon materials, J. Magn. Reson. 234 (2013) 112–124.
[18] N. Bloembergen, S. Shapiro, P.S. Pershan, J.O. Artman, Cross-relaxation in spin systems, Phys. Rev. 114 (1959) 445–459.
[19] K. Takegoshi, S. Nakamura, T. Terao, ^{13}C–^{1}H dipolar-assisted rotational resonance in magic-angle spinning NMR, Chem. Phys. Lett. 344 (2001) 631–637.

[20] M. Weingarth, D.E. Demco, G. Bodenhausen, P. Tekely, Improved magnetization transfer in solid-state NMR with fast magic angle spinning, Chem. Phys. Lett. 469 (2009) 342–348.
[21] Y. Wei, A. Ramamoorthy, 2D ^{15}N–^{15}N isotropic chemical shift correlation established by ^{1}H–^{1}H dipolar coherence transfer in biological solids, Chem. Phys. Lett. 342 (2001) 312–316.
[22] Z. Zhang, H. Chen, C. Wu, R. Wu, S. Cai, Z. Chen, Spatially encoded ultrafast high-resolution 2D homonuclear correlation spectroscopy in inhomogeneous fields, J. Magn. Reson. 227 (2013) 39–45.
[23] K. Takegoshi, S. Nakamura, T. Terao, ^{13}C–^{1}H dipolar-driven ^{13}C–^{13}C recoupling without ^{13}C rf irradiation in nuclear magnetic resonance of rotating solids, J. Chem. Phys. 118 (2003) 2325–2341.
[24] P.L. Gor'kov, E.Y. Chekmenev, C. Li, M. Cotten, J.J. Buffy, N.J. Traaseth, G. Veglia, W.W. Brey, Using low-E resonators to reduce RF heating in biological samples for static solid-state NMR up to 900 MHz, J. Magn. Reson. 185 (2007) 77–93.
[25] B.M. Fung, A.K. Khitrin, K. Ermolaev, An improved broadband decoupling sequence for liquid crystals and solids, J. Magn. Reson. 142 (2000) 97–101.
[26] D. Marion, K. Wüthrich, Application of phase sensitive two-dimensional correlated spectroscopy (COSY) for measurements of ^{1}H–^{1}H spin-spin coupling constants in proteins, Biochem. Biophys. Res. Commun. 113 (1983) 967–974.
[27] R. Fu, X. Wang, C. Li, A.N. Santiago-Miranda, G.J. Pielak, F. Tian, In situ structural characterization of a recombinant protein in native *Escherichia coli* membranes with solid-state magic-angle-spinning NMR, J. Am. Chem. Soc. 133 (2011) 12370–12373.